TAUP 2762/2004
February 1, 2008

The Iancu-Mueller factorization and high energy asymptotic behaviour

M. Kozlov [†] **and E. Levin** [⋆]

HEP Department
School of Physics and Astronomy
Raymond and Beverly Sackler Faculty of Exact Science
Tel Aviv University, Tel Aviv, 69978, Israel

Abstract

We show that the Iancu-Mueller factorization has a simple interpretation in the Reggeon - like technique based on the BFKL Pomeron. The formula for calculating the high energy asymptotic behaviour for the colour dipole-dipole amplitude is proposed which suggests a procedure to calculate this amplitude through the solution to the Balitsky-Kovchegov non-linear equation. We confirm the Iancu - Mueller result that a specific set of enhanced diagrams is responsible for the high energy behaviour for fixed QCD coupling. However, it is argued that in the case of running QCD coupling, this asymptotic behaviour originates from the Balitsky-Kovchegov non-linear equation. A new solution to the non-linear equation is found which leads to a different asymptotic behaviour of the scattering amplitude even for fixed α_S.

[‡] Email: kozlov@tau.ac.il
[⋆] Email: leving@tau.ac.il, levin@mail.desy.de

1 Introduction

Iancu and Mueller in recent papers [1] have suggested a new approach[1] to determine the high energy asymptotic behaviour of the scattering amplitude which goes beyond the non-linear equation (BK equation [3, 4]) of the dense partonic system. In this system the gluon occupation numbers are large, the gluonic fields are strong and such a system enters a new phase of QCD: the colour glass condensate [5, 6, 7, 8] (see also Ref. [9] for a recent review of this approach). The key new element in Iancu-Mueller approach is an attempt to take into account fluctuations in the partonic wave function of the fast moving particle which were neglected in the non-linear equation. These fluctuations could be taken into account by more general approach to CGC related to so called JIMWLK [8] equation, which is functional equation and it is not very practical at the moment. We believe that the Iancu-Mueller approach gives as an opportunity to find more transparent and analytic way to take into account the fluctuations in the partonic wave function.

The main goal of this paper is to show that the Iancu-Mueller approach arises naturally from the Reggeon - like diagram technique [5] based on the BFKL Pomerons [10]. This technique is the well known way of incorporating the fluctuation in the partronic wave function for high energy scattering which leads to the non-linear BK evolution equation [11]. We will review the region of applicability of the non-linear equation for the scattering processes. It was discussed in Ref. [5] (see also Refs.[12, 13, 14]) but it has not been utilized since that time. We show that the Iancu-Mueller result for the scattering amplitude is valid for frozen QCD coupling in a large but limited range of energies, while for running QCD coupling we expect rather the answer obtained in the colour glass condensate.

We concentrate our efforts on understanding dipole-dipole scattering. The main idea of the Iancu-Mueller factorization as well as our approach to this factorization can be illustrated, considering the first so called enhanced diagram (see Fig. 1-a) which describes the fluctuation in the partonic wave function of the incoming fast dipole.

We calculate this diagram in the simple toy - model for the BFKL ladder, namely, assuming for the BFKL Pomeron with the intercept Δ, a simple expression $e^{\Delta y}$, while neglecting any dependence on the size of the interacting dipoles [15]. In addition, we impose the relation $G_1 = g_1 = \Delta$ and $G_2 = g_2 = \frac{\Delta}{N_c^2}$ where N_c is the number of colours. These relations follow directly from the QCD estimates [15, 16], but the most important N_c suppression is the old result of topological expansion [17].

The expression for Fig. 1-a has the form:

$$\begin{aligned} A(\,Fig.\,1-a\,) &= (-1)\,g_1\,g_2\,G_1\,G_2\,e^{\Delta Y}\,\left(\frac{1}{\Delta^2}\,\{\,e^{\Delta Y}\;-\;1\}\;-\;\frac{Y}{\Delta}\right) \\ &= -\,\frac{\Delta^2}{N_c^4}\,e^{\Delta Y}\,\left(\{\,e^{\Delta Y}\;-\;1\}\;-\;\Delta\,Y\,\right) \end{aligned} \tag{1.1}$$

[1]The key ingredients of this approach have been suggested by Mueller and Salam[2] but at that time the approach based mostly on numerical simulations while now we are able to develop analytical methods.

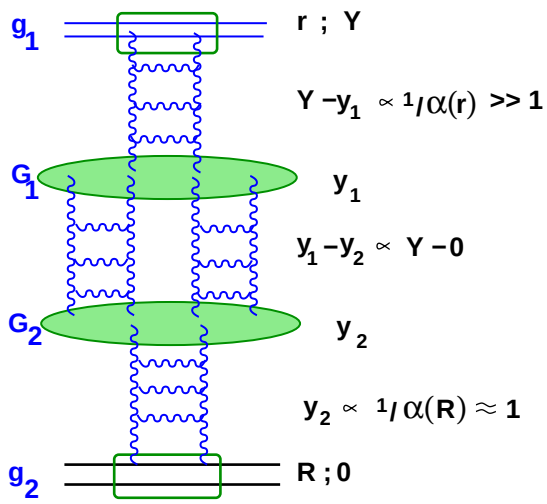

Fig. 1-a

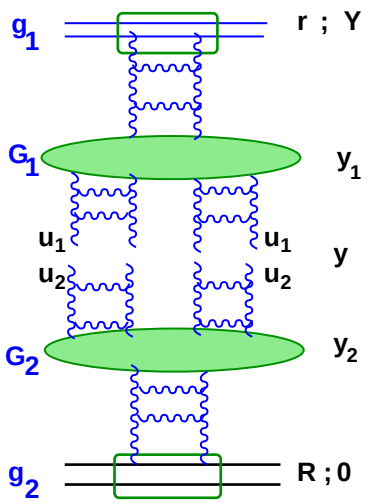

Fig. 1-b

Figure 1: The first enhanced diagram (Fig. 1-a) for dipole-dipole scattering and the Iancu-Mueller factorization for this diagram (Fig. 1-b)

In Eq. (1.1) the sign minus reflects the fact that such diagrams describe shadowing which tames the power-like energy increase $e^{\Delta Y}$, caused by the BFKL Pomeron exchange. For large N_c there exists a region of energy given by the inequality

$$N_c^2 \;\gg\; \frac{1}{N_c^2} e^{\,\Delta Y} \;\geq\; 1 \tag{1.2}$$

in which only the first term in Eq. (1.1) is large (of the order of unity), while all other terms are small. In this region of energy the diagram has a simple form

$$A(\,Fig.\,1-a\,) \;=\; (-1)\,\frac{\Delta^2}{N_c^4}\,e^{2\,\Delta Y} \tag{1.3}$$

The main idea of Iancu and Mueller [1] is to calculate the amplitude of Eq. (1.3) using a different approach, which is presented graphically in Fig. 1-b. This approach is based on the generating function [15, 16, 18]

$$Z(y,u) \;=\; \sum_n \; P_n(Y-y)\,u^n \tag{1.4}$$

where $P_n(y)$ is the probability of having n-dipoles inside the fast dipole. We will show in section 3 that in the simple model, in which we have calculated the diagram of Fig. 1-a, the term in the generating function which is responsible for the amplitude for production of two dipoles (see Fig. 1-b) has the following form:

$$A(Y-y,\gamma) \;=\; 1 - Z(Y-y, u \equiv 1+\gamma) \;=\; (-1)\,\gamma^2\,e^{\Delta(Y-y)}\,\left(e^{\Delta(Y-y)} \;-\; 1\right) \tag{1.5}$$

Therefore, Eq. (1.3) can be written in a different form, namely

$$\begin{aligned} A(\,Fig.\,1-a\,) &= \Delta^2\,(-1)\,A(Y-y,\gamma=1)\,A(y,\gamma=\frac{1}{N_c^2}) \\ &= \Delta^2\,(-1)P_2(Y-y)\,P_2(y)\,\frac{1}{N_c^4} \qquad (1.6) \\ &= \frac{(-1)\,\Delta^2}{4}\,\frac{d^2\,(1-Z(Y-y,1+\gamma))}{(d\gamma)^2}|_{\gamma=0}\,\frac{d^2\,(1-Z(y,1+\gamma/N_c^2))}{(d\gamma)^2}|_{\gamma=0} \end{aligned}$$

Eq. (1.6) leads to the answer, which is not the same as the correct expression for the enhanced diagram given in Eq. (1.1), but it correctly reproduces the leading term (see Eq. (1.3)). The corrections to this term depend on the choice of the value for the rapidity y (see Fig. 1-b) which has only auxiliary meaning. The fact that the generating function Z depends on y is very transparent, since the wave function of the dipole depends on the reference frame. However, the amplitude as a physical observable should not depend on y. It does not depend on y provided

$$\frac{1}{N_c^4}\,e^{\Delta(Y-y)}\;\approx\frac{1}{N_c^2}\;\ll\;1\quad\text{and}\quad\frac{1}{N_c^4}\,e^{\Delta(y)}\;\approx\frac{1}{N_c^2}\;\ll\;1 \qquad (1.7)$$

The choice $y = Y/2$ leads to the estimates that both terms in Eq. (1.7) are of the order of $1/N_c^2 \ll 1$, and is most accurate. This simple seems to justify the choice of the reference frame suggested in Ref. [1].

Formula of Eq. (1.6) is the simplest example of the Iancu-Mueller factorization. In section 3 we will consider in detail a toy-model which we have used here to illustrate the main idea of the Iancu-Mueller factorization. We will show that Eq. (1.6) has a natural generalization which coincides with the direct sum of all enhanced diagrams in the kinematic region given by Eq. (1.2). In section 4 the model result will be generalized for the QCD case to include a dependence on the sizes of the interacting dipoles.

2 Non-linear equation

The non-linear equation [5, 6], the final form of which at fixed impact parameter was suggested by Balitsky [3] and Kovchegov [4], sums all so called 'fan' diagrams (see Fig. 2-a). We would like to repeat here the arguments that led to this equation [5, 6] for the case of the dipole-dipole scattering. The derivation given in Refs. [3, 4] used the fact that the target is a heavy nucleus. As it will be clarified later, the nuclear target indeed enlarges the region of applicability for the non-linear equation, but it is not essential for the saturation in the colour glass condensate domain.

2.1 The first enhanced diagram:

For a deeper understanding of the non-linear equation we start with the calculation of the same enhanced diagram of Fig. 1-a. The gluon 'ladder' shown in this figure is the solution to

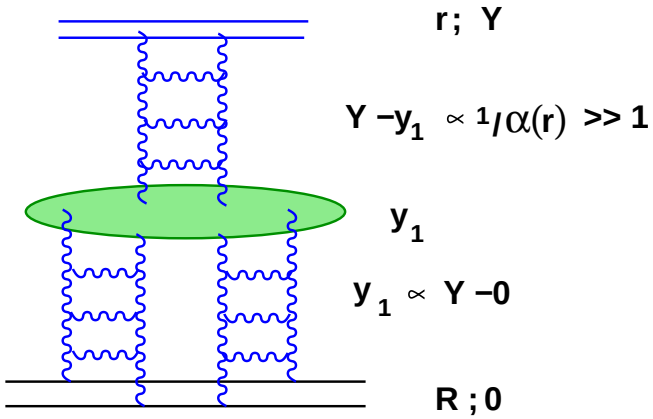

Fig. 2-a

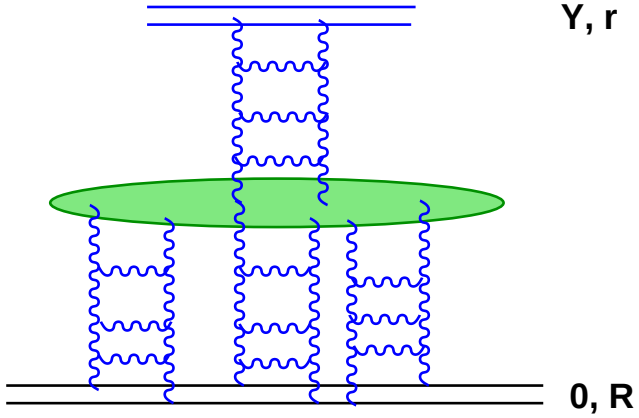

Fig. 2-b

Figure 2: The first 'fan' diagram (Fig. 2-a) for dipole-dipole scattering that is summed by the non-linear evolution equation, and the first diagram that is not included in summation by the non-linear equation (Fig. 2-b)

the BFKL equation [10], which can be written for the dipole (r_1)-dipole(r_2) amplitude in the factorized form [11, 19, 20, 21] (see Fig. 3).

$$N^{BFKL}(r_{1,t}, r_{2,t}; y, q) \;=\; \frac{\alpha_S^2}{4} \tag{2.8}$$

$$\int \frac{d\nu}{2\,\pi\,i}\; D(\nu)\; e^{\omega(\nu)\,y}\, V(r_{1,t}, q; \nu)\, V(r_{2,t}, q; -\nu)$$

with

$$D(\nu) \;=\; \frac{\nu^2}{(\nu^2 + \frac{1}{4})^2} \tag{2.9}$$

and with

$$\omega(\nu) \;\equiv\; \frac{\alpha_S N_c}{\pi}\,\chi(\gamma) \;=\; \frac{\alpha_S N_c}{\pi}\,\left(\,2\,\psi(1) \,-\, \psi(\gamma) \,-\, \psi(1-\gamma)\,\right)\,; \tag{2.10}$$

where $\psi(f) \,=\, d\ln\Gamma(f)/df$, $\Gamma(f)$ is the Euler gamma function, $\gamma \,=\, \frac{1}{2} \,-\, i\,\nu$ and where

$$V(r_{i,t}, q; \nu) \;=\; \frac{2\pi^2}{r_{i,t}\; b(\nu)} \int d^2R\, e^{i\vec{q}\cdot\vec{R}} \left(\frac{r_{i,t}^2}{(\vec{R}_i \,+\, \frac{1}{2}\vec{r}_{i,t})^2\;(\vec{R}_i \,-\, \frac{1}{2}\vec{r}_{i,t})^2} \right)^{\frac{1}{2} - i\,\nu} \tag{2.11}$$

and the following is our notation: $y \,=\, \ln(x_0/x)$; $r_{i.t}$ is the size of the colour dipole "i" and R_i is the position of the center of mass of this dipole. q is momentum transferred along the BFKL Pomeron (see Fig. 3).

The coefficient $b(\nu)$ in Eq. (2.11) is defined in Refs. [19, 21], but we do not need its explicit form in what we discuss below. The only important property of Eq. (2.11) that we will use is

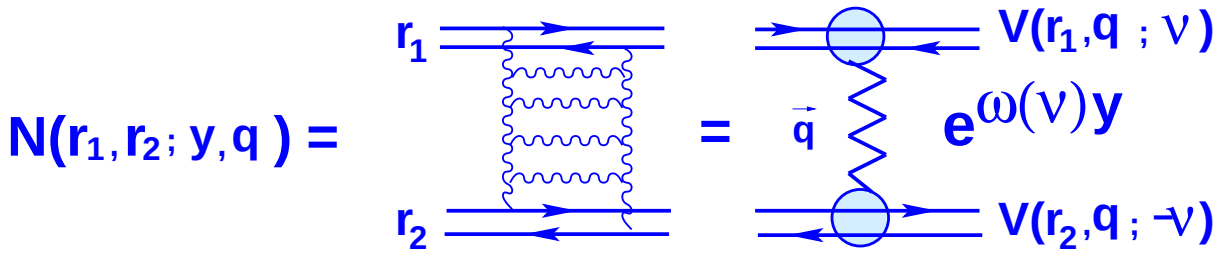

Figure 3: The BFKL Pomeron.

[19, 21]

$$\frac{1}{(2\pi)^2}\int \frac{d^2 r_t}{r_t^2}\, V\left(r_t, q; \nu\right)\, , V\left(r_t, q; -\nu, \right) \;=\; \delta(\nu - \nu') \tag{2.12}$$

The simplest enhanced diagram of Fig. 4 has been given in Ref. [21] and it is equal to

$$N^{enh}\left(r_{1,t}, r_{2,t}; y, q\right) \;=\; -\frac{\alpha_S^4\,\pi^4}{8}\left(\frac{\alpha_S N_c}{2\pi^2}\right)^2 \int d^2k\; d\gamma\, d\gamma_1\; d\gamma_2 \int^Y dy_1 \int^{y_1} dy_2 \tag{2.13}$$

$$V(r_{1,t}, q; \nu) D(\nu)\, e^{\omega(\nu)\,(Y - y_1)}\, G_{3P}(\nu; \nu_1, \nu_2; q, k)\, D(\nu_1)\, D(\nu_2)\, e^{(\omega(\nu_1) + \omega(\nu_2))(y_1 - y_2)} G_{3P}(\nu; \nu_1, \nu_2; q, k)$$
$$D(\nu)\, e^{\omega(\nu)\,(y_2)}\, V(r_{1,t}, q; \nu)$$

where $\gamma_i = 1/2 + i\nu_i$ and the triple Pomeron vertex G_{3P} is calculated in Ref. [21] all details about Eq. (2.13) as well as its explicit derivation, is given.

In spite of the additional complicated integrations over momenta transferred and anomalous dimensions γ_i, appearing in Eq. (2.13), the equation has the same integrations over rapidities as in the simple toy model. Calculating the integrals over y_1 and y_2 and keeping only the maximal power of energy, we reduce Eq. (2.13) to a simpler expression

$$N^{enh}\left(r_{1,t}, r_{2,t}; y, q\right) \;=\; -\frac{\bar{\alpha}_S^4}{32\, N_c^4}\int d^2k\; d\gamma\, d\gamma_1\, d\gamma_2 \int^Y dy_1 \int^{y_1} dy_2\; V(r_{1,t}, q; \nu) \tag{2.14}$$

$$D(\nu)\; G_{3P}(\nu; \nu_1, \nu_2; q, k)\, D(\nu_1)\, D(\nu_2)\, \frac{1}{(\chi(\nu) - \chi(\nu_1) - \chi(\nu_2))^2}\, e^{(\omega(\nu_1) + \omega(\nu_2))\, Y} G_{3P}(\nu; \nu_1, \nu_2; q, k)$$
$$D(\nu)\; V(r_{1,t}, q; \nu)$$

Comparing Eq. (2.14) with Eq. (2.8) one can see that the ratio of these diagrams is of the order of

$$\frac{N(Fig.\ 4)}{N(Fig.\ 3)} \;\propto\; \frac{\bar{\alpha}_S^2}{N_c^2}\, e^{\bar{\alpha}_S\, \chi(0)\, Y} \tag{2.15}$$

At large values of Y this ratio becomes of the order of unity, and to obtain a correct scattering amplitude the enhanced diagrams should be taken into account.

2.2 'Fan' diagrams:

At first sight this discussion leaves no room for a special status of the 'fan' diagrams (see Fig. 2) that are summed by the non-linear equation [3, 4]. Indeed, as was analyzed long ago [5], we cannot expect any suppression of the enhanced diagrams for the fixed QCD coupling, which has been used in the above calculations. However, the situation changes crucially if we consider the scattering amplitude for two dipoles with different sizes (say $r_{1,t} \equiv r \ll r_{2,t} \equiv R$) and we take into account a running QCD coupling. For rather rough estimates let us assume that we can include running α_S by replacing Eq. (2.10) by

$$\omega(\nu) \;=\; \alpha_S(r)\,\chi(\nu)\;. \tag{2.16}$$

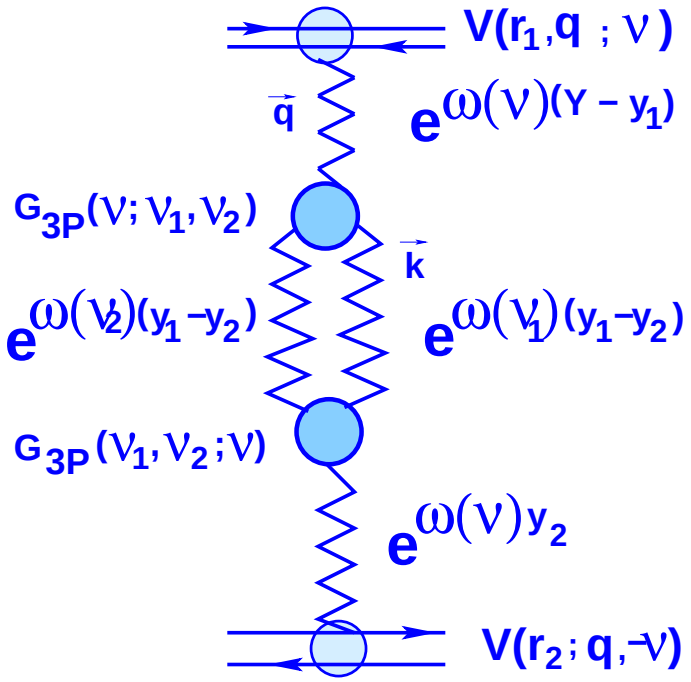

Figure 4: The first enhanced diagram in the Reggeon calculus with the BFKL Pomerons (zigzag lines).

In this case, the typical value for $Y - y_1$ in Eq. (2.13) is of the order of

$$Y \;-\; y_1 \;\sim\; \frac{1}{\alpha_S(r_{1,t})} \;\gg\; 1 \qquad \text{while} \qquad y_2 \;\sim\; \frac{1}{\alpha_S(r_{1,t})} \;\ll\; Y \;-\; y_1 \tag{2.17}$$

If $r_{2,t} \;\approx\; R$ where R is a typical hadron size, $\alpha_S(R) \;\approx\; 1$ and $y_2 \;\approx\; 1$. For such small y we cannot trust the Reggeon like diagrams, but we can replace the enhanced diagram of Fig. 1 or of Fig. 4 by the 'fan' diagram (see Fig. 2). The meaning of such a replacement is that in a 'fan' diagram the interaction of BFKL ladders with the target, is a subject of the non-perturbative QCD approach. Assuming that the BFKL ladders interacts with the target independently (without correlations), we can write the non-linear equation.

Therefore, the non-linear equation is a direct consequence of two physical ideas: (i) the high energy amplitude can be replace by exchange of the BFKL 'ladder'; and (ii) in the first

approximation the correlations can be neglected for the low energy interactions of the BFKL 'ladder' with the target. The last claim has a theoretical justification for a nucleus target [4], here we do not consider the interaction with nucleus.

2.3 Generating functional:

In Ref. [15] A.H. Mueller suggested separating the high energy part of 'fan' diagrams from the low energy part, by introducing the generating functional. This functional has the form:

$$Z\left(Y-y,r;[u_i]\right)\;\equiv\;\sum_{n=1}\int P_n(Y-y,r;r_1,b_1;r_2,b_2;\;\ldots\;r_i,b_i;\;\ldots\;r_n,b_n)\;\prod_{i=1}^{n}u(\vec{r}_i,\vec{b}_i)\,d^2\,r_i\;d^2\,b_i \tag{2.18}$$

where $u(\vec{r}_i)\;\equiv\;u_i$ is an arbitrary function of r_i and b_i. P_n denotes the probability density of finding n dipoles with rapidity y, with transverse size $r_1, r_2, \ldots\; r_i\;\ldots\; r_n$, and with impact parameters $b_1, b_2, \ldots\; b_i\;\ldots\; b_n$ with respect to the mother-dipole, in the wave function of the fast moving dipole of the size r and rapidity $Y\;>\;y$. The functional of Eq. (2.18) satisfies two conditions:

1. At $y\;=\;Y$, $P_1\;=\;\delta^{(2)}(\vec{r}\;-\;\vec{r}_1)$ with $P_{n>1}\;=\;0$. This condition means that at the beginning of the evolution we have one fast moving dipole or, in other words, we sum the 'fan' diagrams which start with the exchange of one BFKL Pomeron. For the functional we have
$$Z\left(Y-y=0,r;[u_i]\right)\;=\;u(r)\;; \tag{2.19}$$

2. At $u_i=1$
$$Z\left(Y-y,r;[u_i=1]\right)\;=\;1\;; \tag{2.20}$$
Eq. (2.20) expresses the physical meaning of the functional:the sum over all probabilities is equal to unity.

This functional sums all 'fan' diagrams (see Fig. 5), and the simple linear functional equation can be written for it [14]:

$$\frac{\partial Z\left(Y-y,r,;[u_i]\right)}{\partial\bar{\alpha}_S\;y}\;=\;-\;\int\;d^2r_i\,u(r_i)\,\omega(r_i)\;\frac{\delta}{\delta u_i}\;Z\left(Y-y,r;[u_i]\right) \tag{2.21}$$
$$+\;\int\;d^2\,r_i\;d^2\,r'\,u(r_i)\,u(\vec{r}_i-\vec{r}')\;\frac{r'^2}{r_i^2\,(\vec{r}_i-\vec{r}')^2}\;\;\frac{\delta}{\delta u(r')}\;Z\left(Y-y,r;[u(r'),u_i]\right)$$

where

$$\omega(r)\;=\;\frac{1}{2\pi}\int\;d^2\,r'\;\frac{r^2}{r_i'^2\,(\vec{r}-\vec{r}')^2}\;, \tag{2.22}$$

the notation $\delta/\delta u_i$ is used for the functional derivative.

The physical meaning of each term is clear: the first one describes a probability for the BFKL Pomeron to propagate from rapidity y to rapidity $y+dy$ without any decay, while the

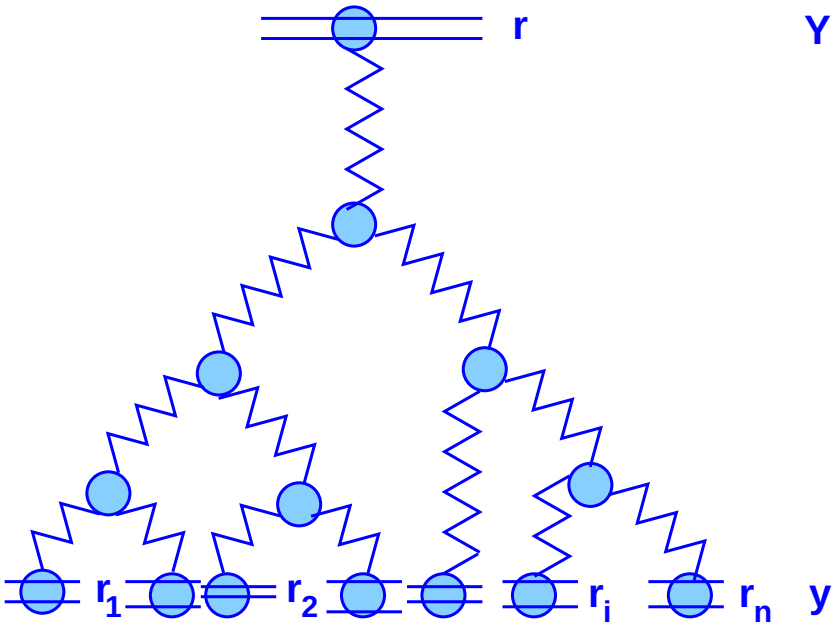

Figure 5: The 'fan' diagrams that are summed by the generating functional. Zigzag lines denote the BFKL Pomerons.

second term accounts for the possibility for decay of one dipole to two dipoles or, in other words, it takes into account the triple BFKL Pomeron vertices.

A general property of Eq. (2.21), is that a solution to this equation can be written as a function of a single variable $u(y)$. Rewriting $\partial Z/\partial y$ as $\partial Z/\partial y = \int d^2r\ (\delta Z/\delta u(r))\ (\partial u(r)/\partial y)$ and using the initial condition of Eq. (2.19) one obtains a non-linear equation [15]:

$$\frac{dZ\left(Y-y,r;[u_i]\right)}{d\bar{\alpha}_S\ Y} \;=\; -\omega(r)\ Z\left(Y-y,r;[u_i]\right) \tag{2.23}$$

$$+\int d^2\,r'\ \frac{r^2}{r'^2\,(\vec{r}\,-\,\vec{r}')^2}\ Z\left(Y-y,r';[u_i]\right)\ Z\left(Y-y,\vec{r}\,-\,\vec{r}');[u_i]\right)\ .$$

Eq. (2.21) and Eq. (2.23) solve the problem of finding the probability to produce a number of dipoles of different sizes at rapidity y, from the single fast moving dipole at rapidity Y. This probability is independent of the target. Assuming that all produced dipoles interact with the target independently (without correlations), we can calculate the resulting scattering amplitude for the 'fan' diagram (see Fig. 2). As was proved in Ref.[4], this amplitude is equal to

$$N\left(Y,r;[\gamma(r_i,b_i)]\right) \;=\; 1 \;-\; Z\left(Y,r,b_t;[\gamma(r_i,b_i)+1]\right)\ . \tag{2.24}$$

where $-\gamma(r_i,b_i)$ is the amplitude of the interaction of the dipole of size r_i, at impact parameter b and at $y=0$ with the target.

2.4 The Iancu-Mueller factorization and enhanced diagrams:

The Iancu-Mueller approach to calculations of the enhanced diagrams contribution to the scattering amplitude is shown in Fig. 6. We need therefore

(i) to calculate the amplitude of production of n-dipoles of the different sizes, that are produced by both colliding dipoles with sizes r and R in Fig. 6;

(ii) to multiply the product of these amplitudes by $\gamma(r_i, r'_i)$ for each pair;

(iii) to integrate over all r_i, b_i and r'_i, b'_i.

Summing over all possible numbers of the interacting dipoles give us the amplitude. This procedure leads to the following formula (see Fig. 6):

$$N\left(r, R, Y; b\right) \;=\; \sum_{n=1}^{\infty} \int \prod_{i=1}^{n} d^2 b_i \; b'_i \prod_{i=1}^{n} d^2 r_i \; d^2 \, r'_i \;\; \tilde{\gamma}(r_i, \vec{b} - \vec{b}_i; r'_i, b'_i) \tag{2.25}$$

$$N_n \left(r, Y - y; r_1, \vec{b} - \vec{b}_1; r_2, \vec{b} - \vec{b}_2; \; \ldots \; r_i \, \vec{b} - \vec{b}_i; \ldots \; r_n \; \vec{b} - \vec{b}_n\right) \;\; N_n \left(R, y; r'_1, b'_1; r'_2, b'_2; \; \ldots \; r'_i, b'_i \; \ldots \; r'_n, b'_n\right)$$

where N_n is the general term of expansion of the amplitude given by Eq. (2.24)

$$N\left(Y, r; [\gamma(r_i, b_i)]\right) \;=$$

$$- \sum_{n=1} \prod_{i=1}^{n} d^2 \, r_i \, d^2 \, b_i \;\; \gamma(r_i, b_i) N_n \left(r, Y; r_1, b_1; r_2, b_2 \; \ldots \; r_i, b_i; \; \ldots \; r_n, b_n\right) \;\; . \tag{2.26}$$

In Eq. (2.26) we view the scattering amplitude $N\left(Y, r; [\gamma(r_i, b_i)]\right)$ as a generating functional with respect to arbitrary functions $\gamma(r_i)$. To obtain the scattering amplitude for the particular process we have to replace functions $\gamma(r_i)$ by $\tilde{\gamma}(r_i, R)$ where $\tilde{\gamma}(r_i, R) = -A(dipole - target)$ where A is the amplitude of the dipole - target interactions at low energies with sizes r_i and R, respectively.

Comparing Eq. (2.24) and Eq. (2.26) one can see that N_n can be calculated as

$$N_n \left(r, Y, b, r_1, b_1; r_2, b_2; \; \ldots \; r_i, b_i; \; \ldots \; r_n, b_n\right) \;=\; \frac{1}{n!} \prod_{i=1}^{n} \frac{\delta}{\delta \gamma_i} \; \left(\; 1 \;\; - \;\; Z\left(Y, r; [\gamma(r_i, b_i) + 1]\right) \; \right) |_{\gamma_i = 0} \; . \tag{2.27}$$

As we have discussed, the artificial rapidity y cancels in the product of Eq. (2.25).

In principle Eq. (2.25) solves the problem of calculating the scattering amplitude, if we can find the expression for $\tilde{\gamma}(r_i, r'_i)$. Comparing Eq. (2.8) and Eq. (2.13) and taking into account the completeness relation of Eq. (2.12) we obtain that

$$\tilde{\gamma}(k_i, k'_i; r_i, r'_i) \;=\; (-1) \; \delta^{(2)}(\vec{k}_i - \vec{k}'_i) \; \delta^{(2)}(\vec{r}_i - \vec{r}'_i) \; \frac{\bar{\alpha}_S^2 \, \pi^3}{N_c^2} \, \frac{1}{D(\nu)} \, \frac{1}{r_i^2} \tag{2.28}$$

Returning to the impact parameter representation we have Eq. (2.28) in the form

$$\tilde{\gamma}(\vec{b}_i, \vec{b}'_i; r_i, r'_i) \;=\; (-1) \; \delta^{(2)}(\vec{r}_i - \vec{r}'_i) \; \delta^{(2)}(\vec{b}'_i - \vec{b}_i) \; \frac{\bar{\alpha}_S^2 \, \pi^3}{N_c^2} \, \frac{1}{D(\nu)} \, \frac{1}{r_i^2} \tag{2.29}$$

We recall that $\bar{\alpha}_S = N_c \, \alpha_S / \pi$.

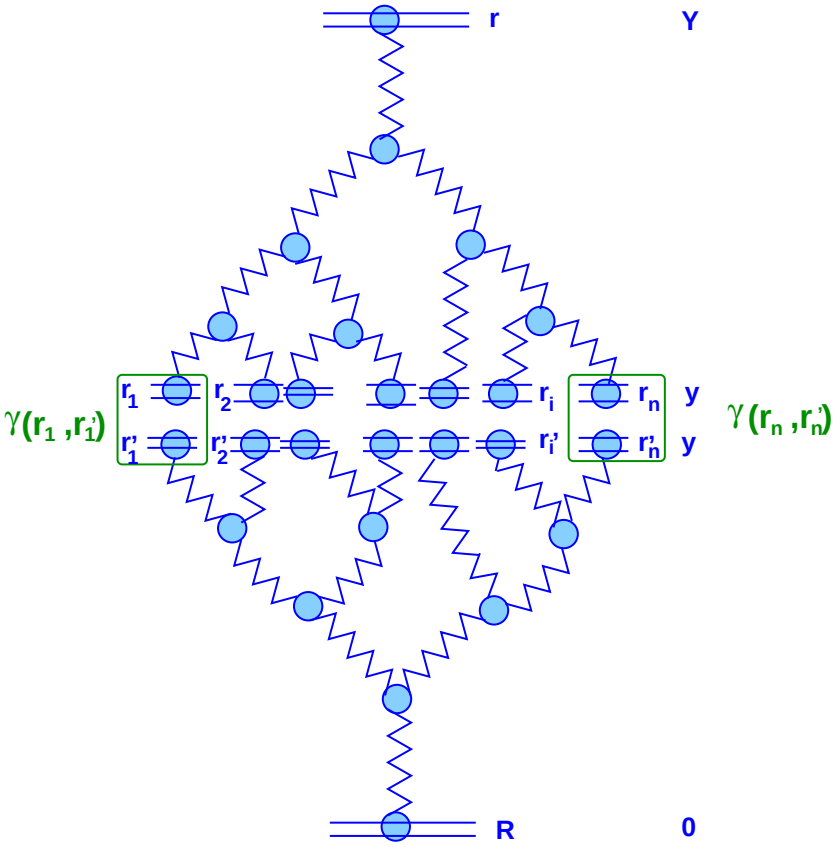

Figure 6: The enhanced diagrams that are summed by the Iancu-Mueller approach. Zigzag lines denote the BFKL Pomerons.

We can clarify the physical meaning of Eq. (2.28) and Eq. (2.29) by considering the first term in Eq. (2.27), which corresponds to the single BFKL Pomeron exchange. This term is equal which corresponds to the

$$N\left(Y-y,r,q;[\gamma(r_1)]\right) \;=\; \int d^2r_1 N^{BFKL}\left(Y-y,r,r_1;q\right)\;\gamma(r_1) \tag{2.30}$$

Choosing $\gamma(r_1)=\nu$ and $\gamma(r'_1)=\tilde{\gamma}(q;r_1,r'_1)/\nu$, one can see that Eq. (2.26) could be rewritten in the form

$$\begin{aligned} N^{BFKL}\left(Y,r,R;q\right) &= -\int d^2r_1\, d^2r'_1 N\left(Y-y,r,b;[\gamma(r_1)]\right)\;N\left(y,R,q;[\gamma(r'_1)]\right) \qquad (2.31)\\ &= -\int d^2r_1\, d^2r'_1 N^{BFKL}\left(Y-y,r,r_1;q\right)\;\nu\, N^{BFKL}\left(y,R,r'_1;q\right)\;\frac{\tilde{\gamma}(q;r_1,r'_1)}{\nu}\\ &= -\int d^2r_1\, d^2r'_1 N^{BFKL}\left(Y-y,r,r_1;q\right)\;N^{BFKL}\left(y,R,r'_1;q\right)\;\tilde{\gamma}(q;r_1,r'_1) \end{aligned}$$

In the last equation we use the completeness of the BFKL vertex functions $V(r,q,\nu)$ (see Eq. (2.12)) and the explicit form of Eq. (2.28) for $\tilde{\gamma}(q;r_1,r'_1)$, to take the integrals over r_i and r'_i. Eq. (2.31) gives the main formula that allows us to reduce the product of two functional to the exchange of the BFKL Pomeron and, therefore, to the Reggeon -like diagram technique.

This formula together with Eq. (2.25) and Eq. (2.27) leads to the calculation of the scattering amplitude in the Iancu-Mueller approach. However, before performing a calculation

using Eq. (2.25) and Eq. (2.27) we would like to clarify our approach using a simple model suggested in Ref. [15].

3 The Iancu-Mueller factorization in a toy model

We have used this model in the introduction to illustrate the main points of our approach to the Iancu-Mueller factorization. In the toy model, the probability for the dipole to decay in two dipoles is a constant (ω_0), which is equal to the probability for a dipole to survive without producing another dipole. In other words, in the framework of the Reggeon -type diagram technique, the intercept of Pomeron is equal to G_{3P} - vertex, and both are equal to ω_0. In this model we also neglect the fact that we have dipoles of different sizes, and therefore the generating functional of Eq. (2.18) reduces to a generating function

$$Z(Y-y,u) \;=\; \sum_{n=1} \; P_n \; u^n \tag{3.32}$$

with two initial and boundary conditions:

$$\text{At y = Y}: \quad Z(Y-y=0,u) \;=\; u \;; \tag{3.33}$$

$$\text{At u =1}: \quad Z(Y-y,u=1) \;=\; 1; \tag{3.34}$$

Eq. (2.21) reduces to (see Refs. [15, 14])

$$-\;\frac{\partial\, Z(y,u)}{\partial y} \;=\; -\omega_0\;(u(1-u))\;\frac{\partial\, Z(y,u)}{\partial u} \tag{3.35}$$

which has the solution

$$Z(Y-y,u) \;=\; \frac{u}{1\;+\;(\,e^{\omega_0\,(Y-y)}-\,)\,(1\;-\;u)}\;. \tag{3.36}$$

Using Eq. (2.24) one obtains

$$N(Y-y,\gamma) \;=\; -\;\frac{\gamma\, e^{\omega_0\,(Y-y)}}{1\;+\;\gamma\;(\;e^{\omega_0\,(Y-y)}\;-\;1\,)} \tag{3.37}$$

Eq. (3.37) together with a natural reduction of Eq. (2.29) to

$$\tilde{\gamma} \;\equiv\; \gamma_{SM} \;=\; (-1)\,\frac{\bar{\alpha}_S^2\,\pi^3}{N_c^2} \tag{3.38}$$

allows us to use Eq. (2.25) to estimate the high energy asymptotic behaviour of the scattering amplitude, in this simple model. However, we suggest a more compact formula than Eq. (2.25), namely,

$$N(Y) \;=\; \frac{1}{2\,\pi\,i}\oint_{C_1}\;\frac{d\nu}{\nu}\;N(Y-y,\gamma_{SM}\,\nu)\,N(y,\frac{1}{\nu})\;; \tag{3.39}$$

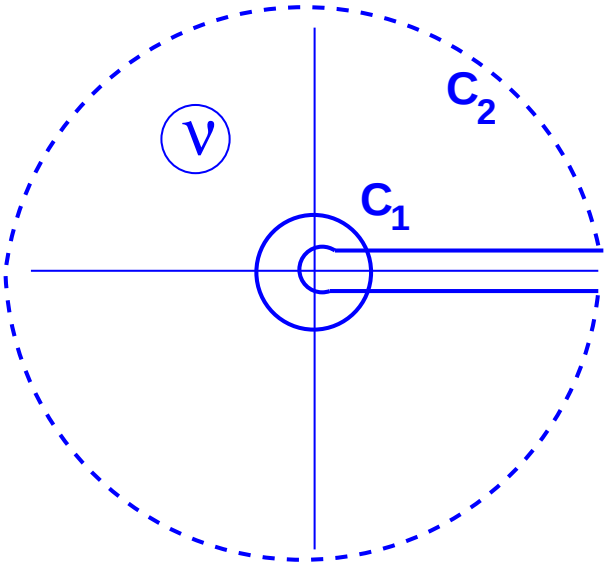

Figure 7: Complex ν plane and contours for integration over ν in Eq. (3.39) and Eq. (4.53) .

where the integration contour is a circle with the unit radius around $\nu = 0$ (see contour C_1 in Fig. 7). Expanding the functions Z with respect to ν and $1/\nu$ one can prove in the case of our simple model that Eq. (3.39) is equivalent to Eq. (2.25).

Taking the integral of Eq. (3.39) explicitly we obtain the answer

$$N(Y) \;=\; = \; \frac{\frac{\bar{\alpha}_S^2\,\pi^3}{N_c^2}\,e^{\omega_0\,Y}}{1\;+\;\frac{\bar{\alpha}_S^2\,\pi^3}{N_c^2}\,\left(\,e^{\omega_0\,(Y-y)}\;-\;1\,\right)\,\left(\,e^{\omega_0\,y}\;-\;1\,\right)} \tag{3.40}$$

where γ_{SM} is given by Eq. (3.38). On can see that Eq. (3.40) leads to

$$\lim_{Y\gg 1} N(Y) \;\to\; 1\;-\;\frac{\bar{\alpha}_S^2\,\pi^3}{N_c^2}\,e^{-\omega_0\,Y}\;+\;O\left(\frac{\bar{\alpha}_S^2\,\pi^3}{N_c^2}\,e^{-\omega_0\,Y/2}\right) \tag{3.41}$$

4 High energy asymptotic behaviour of the scattering amplitude

In this section we return to the general expression for the Iancu-Mueller factorization given by Eq. (2.25) and Eq. (2.27). We would like to calculate the high energy asymptotic behaviour based on our experience with the simple model, that has been discussed in the previous section.

We start with discussion of dipole-dipole amplitude in the simplified model for the BFKL kernel, namely, assuming that

$$\omega(\gamma) \;=\; \frac{\alpha_S\,N_c}{\pi}\,\begin{cases} \frac{1}{\gamma} & \text{for } r^2\,Q_s^2\;<\;1\,; \\ \\ \frac{1}{1\,-\,\gamma} & \text{for } r^2\,Q_s^2\;>\;1\,; \end{cases} \tag{4.42}$$

instead of the general BFKL kernel given by Eq. (2.10). In Eq. (4.42) Q_s denotes the saturation momentum. It is shown in Ref.[22] that Eq. (4.42) sums double log contributions of the order of $(\alpha_S Y \ln(r^2\,\Lambda^2))^n$ in the kinematic region of perturbative QCD, namely, $r^2\,Q_s^2 < 1$, while in the saturation region ($r^2\,Q_s^2 > 1$) it takes into account large terms of $(\alpha_S \ln(r^2\,Q_s^2))^n$ -type. In section 4.3 we will return to discussion of the general kernel of Eq. (2.10).

4.1 Fixed α_S:

4.1.1 Generating functional for the Balitsky - Kovchegov scattering amplitude:

We calculate the high energy asymptotic behaviour of the scattering amplitude using our experience with the simple toy model, and the fact that amplitude $N\,(Y, r, b; [\gamma(r_i)])$ has been found in Ref. [22]. We will show that a direct generalization of Eq. (3.39) leads to the high energy amplitude that has been proposed in the Iancu-Mueller paper [1], namely,

$$N(Y, r_1, r_2; b) \implies 1 - e^{-\frac{1}{2}\,c\,(Y - Y_0)^2} \tag{4.43}$$

where coefficient c determines the asymptotic behaviour of the solution to the Balitsky-Kovchegov non-linear equation. This behaviour was found in Ref. [22] and it has the form

$$N^{BK}(Y, r_1; b) \implies 1 - e^{-\,c\,(Y - Y_0)^2} \tag{4.44}$$

with $c = 2\,\bar{\alpha}_S^2$.

The first problem that we need to solve, is to build the generating functional for the amplitude (see Eq. (2.26)), based on the solution given in Ref. [22].

$$\boldsymbol{r_t \;<\; 1/Q_s(Y - y, b)}$$

As was shown in this paper, the solution for the short distances ($r_t\,Q_s < 1$) is the single BFKL Pomeron, and, therefore, the generating function for the scattering amplitude at these distances is

$$N_{sd}\,(Y - y, r_1, b; [\gamma(r_i)]) \;=\; \int d^2 r_i\;\gamma(r_i)\;N^{BFKL}((Y - y, r_1, r_i, b) \tag{4.45}$$

$$\boldsymbol{r_t \;>\; 1/Q_s(Y - y, b)}$$

For long distances, the solution for the interaction of the dipole (r_1) with the dipole (r_i) can be written in the form [22]:

$$N\,(Y - y, r_1, r_i; b) \;=\; 1 \;-\; e^{-\phi(z)} \tag{4.46}$$

where

$$z \;=\; \ln\left(r_1^2\, Q_s^2\right) \;=\; 4\bar{\alpha}_S\,(Y-y) \;-\; \ln(r_i^2/r_1^2) \;+\; 2\,\beta(b) \tag{4.47}$$

for the kernel of Eq. (4.42). $\beta(b) \;=\; 2\,\ln S(b)$ in this approach, where $S(b)$ is given by the impact parameter dependence of the Born approximation amplitude for this interaction (see Ref. [22] for details).

Function ϕ is defined [22] by

$$z \;=\; \sqrt{2}\int_{\phi_0}^{\phi} \frac{d\,\phi'}{\sqrt{\phi' \;+\; e^{-\phi'} \;-\; 1}} \tag{4.48}$$

where the value of ϕ_0 should be found by matching the solution with Eq. (4.46) at $r_1 = 1/Q_s$.

Assuming that ϕ_0 is small we obtain from Eq. (4.48) that for $z < 1$

$$N\,(Y-y, r_1, r_i; b) \;=\; \phi_0\, e^{\frac{1}{2}\,z} \tag{4.49}$$

Comparing Eq. (4.49) with the functional of Eq. (4.45) and recalling that $N^{BFKL} \;\to\; exp[\frac{1}{2}z]$ for r_1 approaching $1/Q_s$, we obtain that in the region of long distances, but for r_1 close to $1/Q_s$, that the generating functional for scattering amplitude has the form:

$$N_{ld}\,(Y-y, r_1, b; [\gamma(r_i)]) \;\;=\;\; \int\; d^2 r_i\;\gamma(r_i)\; e^{-\frac{1}{2}\,\ln(r_i^2)} \tag{4.50}$$

Using Eq. (4.50) and Eq. (4.48) we can see that in the region of large z ($Y - y \;\gg\; \ln(1/r^2) \;\gg\; 1$) the generating functional is

$$N_{ld}\,(Y-y, r_1, b; [\gamma(r_i)]) \;\;=\;\; 1 \;-\; e^{-\frac{1}{2}\left(\,\frac{z}{2}+\Phi[\gamma(r_i)]\,\right)^2} \tag{4.51}$$

with the functional $\Phi([\gamma(r_i)])$ defined as

$$\Phi([\gamma(r_i)]) \;\;=\;\; \ln\left(\int\; d^2\, r_i\, e^{-\frac{1}{2}\ln(1/r_i^2)}\;\gamma(r_i)\right) \tag{4.52}$$

where z is defined by Eq. (4.47).

The accuracy of Eq. (4.51) is not very high and we cannot guarantee the value of the constant in front of the exponent in Eq. (4.51).

4.1.2 Dipole-dipole scattering amplitude in Iancu - Mueller approach:

To calculate the dipole-dipole scattering amplitude we would like to generalize Eq. (3.39). We replace $\gamma(r_i)$ by ν, while we choose $\gamma(r_i') = \tilde{\gamma}(r_i, r_i')/\nu$ (see Eq. (2.29)).

Using these functions γ we can rewrite Eq. (2.25) in the form of Eq. (3.39), namely,

$$N\,(r, R, Y; b) \;\;=\;\; \frac{1}{2\,\pi\, i}\oint_{C_2} \frac{d\nu}{\nu}\, N\,(Y-y, r, b; [\nu])\;\; N\,(y, R, b; [\tilde{\gamma}(r_i, r_i')/\nu]) \tag{4.53}$$

where we deform contour C_1 to contour C_2 (see Fig. 7). In Eq. (4.53) we use r and R instead of r_1 and r_2 denoting the sizes of colliding dipoles.

Substituting Eq. (4.51) in this equation we obtain the resulting expression

$$N\,(r,R,Y;b) \;\; = \tag{4.54}$$

$$\frac{1}{2\,\pi\,i}\oint_{C_2}\frac{d\nu}{\nu}\,\left(\,1\;\;+\;\;e^{-\frac{1}{2}\left(\,\left(\,\frac{z\,(Y-y,r)}{2}+\Phi[\nu]\,\right)^2+\left(\,\frac{z\,(y,R)}{2}+\Phi[\tilde{\gamma}(r_i,r_i')/\nu]\,\right)^2\right)}\,\right)$$

In Eq. (4.54) we denote the sizes of interacting dipoles by r and R instead of r_1 and r_2. As we have seen in toy model example, the contour of integration is situated between all singularities of two amplitudes in Eq. (4.54). Due to this fact the contributions such as

$$-e^{-\frac{1}{2}\left(\,\frac{z\,(Y-y,r)}{2}+\Phi[\gamma(r_i)]\,\right)^2}\qquad\text{and}\qquad-\,e^{-\frac{1}{2}\left(\,\frac{z\,(y,R)}{2}+\Phi[\gamma(r_i)]\,\right)^2}$$

are equal to zero since they have singularity outside of contour C_2. Since the integral over the large circle (see dotted line in Fig. 7) is equal to zero, Eq. (4.54) can be rewritten as follows

$$N\,(r,R,Y;b) \;\; = \tag{4.55}$$

$$1\;\;+\;\;\frac{1}{\pi}\,\left(1-e^{2\pi^2}\right)\,\int_{-\infty}^{+\infty}\,d\,l\;e^{-\frac{1}{2}\left(\,\left(\,\frac{z\,(Y-y,r)}{2}+\,l\,+\,\chi\,\right)^2+\left(\,\frac{z\,(y,R)}{2}\,-\,l\,+\,\chi[\tilde{\gamma}(r_i,r_i')]\,\right)^2\,\right)}$$

We are not sure of the value of the coefficient in front of the integral, but we wrote it explicitly, to show that the second term is negative. In Eq. (4.55) we extract the variable ν from both Φ's and use the notation $l\,\equiv\,\ln\nu$. Taking the integral over l explicitly one obtains

$$N\,(r,R,Y;b) \;\;=\;\; 1\;\;-\;\;e^{-\,\frac{1}{16}\,z^2(Y,r,R)} \tag{4.56}$$

where

$$z(Y,r,R) \;\;=\;\; 4\,\bar{\alpha}_S\,Y\;\;-\;\;\ln(R^2/r^2) \tag{4.57}$$

Eq. (4.56) reproduces the result of the Iancu and Mueller paper [1] (with numerical coefficients of our simplified model for the BFKL kernel given by Eq. (4.42)) and it does not contain any variable related to the fictional dipoles with rapidity y as well as rapidity y itself.

The sum of 'fan' diagrams leads to the answer [22]

$$N_{fan}\,(r,R,Y;b) \;\;=\;\; 1\;\;-\;\;e^{-\,\frac{1}{8}\,z^2(Y,r,R)} \tag{4.58}$$

which is much closer to unity than the correct answer given by Eq. (4.56). In the case of fixed QCD coupling our calculations as well as the Iancu and Mueller ones, show that the non-linear BK equation is not able to describe the physics of the dipole-dipole interactions, even when dipoles have quite different sizes (say $R\;\gg\;r$).

4.2 Running α_S:

It is not theoretically clear how to include the running QCD coupling in this approach, mostly because we do not know how to write the BFKL kernel for running QCD coupling. However, for short distances in the pQCD phase ($r^2\,Q_s^2 \leq 1$) we know that α_S in the BFKL equation depends on the size of the scattered dipole [5, 24, 25]. This dependence leads to the saturation scale $Q_s(Y) \;\propto\; e^{\sqrt{cY}}$ and to the geometric scaling behaviour versus the variable $r^2Q_s^2$ (at least within the semi-classical accuracy) [5, 24].

Inside the saturation region ($r^2\,Q_s^2 \gg 1$) we can assume that the running α_S is frozen at the saturation scale [13]. This assumption appears natural from the point of view that physics of saturation is determined by one scale: the saturation momentum [5, 6, 7]. Indeed, it was shown in Ref. [13], that this assumption leads to the geometrical scaling [23] in the saturation region, making our hypothesis self-consistent and providing the natural matching with the pQCD region.

In the framework of this assumption we obtain the same solution given by Eq. (4.46) but with a new variable z, namely

$$z \;=\; \ln\left(Q_s^2\;r_1^2\right) \;=\; 2\bar{\alpha}_S(Q_s^2)\,(Y\;-\;y)\;-\;\ln(r_i^2/r_1^2)\;+\;2\beta(b)\;. \tag{4.59}$$

In Eq. (4.59) we use the expression for the saturation scale in the case of running α_S obtained in Refs. [5, 24, 13]. We would like to recall that in Refs. [5, 24, 13] instead of factor 2 in the second line stands $(1/2)\,d\chi(\gamma)/d\gamma|_{\gamma=\gamma_{cr}}$, where γ_{cr} is the solution to the equation $\chi(\gamma_{cr})/(1-\gamma_{cr}) = -d\chi(\gamma)/d\gamma|_{\gamma=\gamma_{cr}}$. However, in DLA the BFKL kernel $\chi(\gamma)$ is so simple that $\gamma_{cr} = 1/2$ and $(1/2)\,d\chi(\gamma)/d\gamma|_{\gamma=\gamma_{cr}} = 2$. In section 4.3 we will discuss the general form of the BFKL kernel and all these numerical factors will reappear in our calculations.

Finally, after performing the same calculation as has been discussed above, we obtain the same formula of Eq. (4.56) but with

$$\begin{aligned} Z(Y,r,R) \;&=\; 2\bar{\alpha}_S(Q_s(Y-y))\,(Y-y)\;+\;2\bar{\alpha}_S(Q_s(y))\,y\;-\;\ln(R^2/r^2) \\ &=\; \frac{8\,N_c}{b}\left(\sqrt{Y-y}\;+\;\sqrt{y}\right)\;-\;\ln(R^2/r^2)\;; \end{aligned} \tag{4.60}$$

The minimum of $Z(Y,r,R)$ occurs at $y = 0$ or at $y = Y$. The case $y = 0$ in our notation corresponds to the 'fan' diagrams of Fig. 2-a type (see also Fig. 5), if we assume that $R > r$. We indeed assumed this, considering $\ln(r_i/r) > 0$ and $\ln(R/r_i') > 0$ when we tried to justify the generating functional approach for the 'fan' diagrams. As has been discussed in section 2.2 (see also [5]), the selection of the 'fan' diagrams was defined for the dipole sizes less than $1/Q_s$.

Therefore, only the solution for $y = 0$ can match the amplitude at $r < 1/Q_s$. Finally, our calculations support the principal idea of the non-linear equation that in the case of running QCD coupling it describes the interaction of the dipoles with different sizes. However, this conclusion is based on an additional assumption that the running QCD coupling is frozen on the saturation scale.

As was argued in Ref. [25], in the approach given by Eq. (4.42), it seems natural to assume that α_S depends on the size of produced dipole. Indeed, in this case we expect that the size of the produced dipole (r' or $|\vec{r}-\vec{r}'|$ in Eq. (2.23)) is smaller than the size of the scattered dipole but larger than $1/Q_s$ inside the saturation domain [22, 25]. Therefore, we can replace

$$\alpha_S \int \frac{r^2}{r'^2\,(\vec{r}-\vec{r}')^2} \;\to\; \pi \int_{1/Q_s^2}^{r^2} \alpha_S(r')\,\frac{dr'^2}{r'^2} \;+\; \pi \int_{1/Q_s^2}^{r^2} \alpha_S(|\vec{r}-\vec{r}'|)\,\frac{d\,(\vec{r}-\vec{r}')^2}{(\vec{r}-\vec{r}')^2}\;. \tag{4.61}$$

Introducing a new function $\tilde{N}(\xi,y) \;=\; \int_\xi^{\xi_s} \alpha_S(\xi')\,d\xi'\; N(xi',y)$ where N is the dipole scattering amplitude and $\xi \;=\; \ln(1/(r^2\Lambda^2))$ and $\xi_s \;=\; \ln(Q_s^2/\Lambda^2)$, we can rewrite the Balitsky-Kovchegov equation in the following way

$$-\;\frac{d^2\tilde{N}(\xi,y)}{dy\,d\,\xi} \;=\; \frac{2\,C_F}{\pi}\left(\alpha_S(\xi)\,\tilde{N} \;+\; \tilde{N}(\xi,y)\,\frac{d\tilde{N}(\xi,y)}{d\xi}\right) \tag{4.62}$$

which is a direct generalization of Eq.(2.13) in Ref. [22]. Replacing $N(\xi,y)$ by function $\phi(\xi,y)$ using $N = 1 - e^{-\phi(\xi,y)}$ one can see that Eq. (4.62) reduces to

$$\frac{d\,\phi}{dy} \;=\; \frac{2\,\alpha_S(\xi)\,C_F}{\pi}\,\tilde{N} \tag{4.63}$$

Assuming that ϕ increases moving inside of the saturation region , one can see that $\tilde{N}$ approaching

$$\tilde{N} \;\longrightarrow\; \frac{4\pi}{b}\,\ln\left(\frac{\xi_s}{\xi}\right) \tag{4.64}$$

Substituting Eq. (4.64) in Eq. (4.63) and integrating with respect to y using the explicit expression for ξ_s ($\xi_s \;=\; \sqrt{\frac{16\,N_c}{\pi\,b}}\;y$) we obtain

$$\phi(\xi,y) \;=\; \frac{8\,\alpha_S(\xi)\,C_F}{b}\;\{\,y\;\left(\frac{1}{2}\,(\ln y - 1) + \ln\sqrt{\frac{16\,N_c}{\pi\,b}} \;-\; \ln\xi\right) \;+\; C(\xi)\,\} \tag{4.65}$$

Function $C(\xi)$ in Eq. (4.65) can be found from the condition that $\phi(\xi = \xi_s) = Const$. The final answer has the form [2]

$$\phi(\xi,y) \;=\; \frac{\alpha_S(\xi)}{2\,\pi}\,\left(\xi_s^2\,(\ln(\xi_s/\xi) - 1) + \xi^2\right) \tag{4.66}$$

One can see that this solution does not show the geometric scaling behaviour. However, if ξ is close to ξ_s Eq. (4.66) degenerates into geometrical scaling behaviour within accuracy $\ln(Q_s^2\,r^2)/\ln(Q_s^2/\Lambda^2)$. Therefore, this solution is not worse that the one discussed before with the exact geometrical scaling behaviour.

[2] This solution is very similar to the solution obtained in Ref.[25] but it has an extra factor $\alpha_S(\xi)$. It should be stressed that only with this factor this solution could be matched with the geometrical scaling solution in the pQCD region ($r^2Q_s^2 < 1$).

Repeating the same calculation as in section 4.1 but with the solution given by Eq. (4.66) we obtain the behaviour

$$N\left(r,R,Y;b\right) \;=\; 1 \;-\; e^{-\phi(Y-y,r)-\phi(y,R)} \tag{4.67}$$

One can see that minimum of the sum of ϕ's occurs at

$$\xi_s^2(y_{min}) = \xi^2(r)\,\left(\frac{\xi_s^2(Y)}{\xi^2(R)}\right)^{\frac{\alpha_S(r)}{\alpha_S(R)}} \tag{4.68}$$

where we used obvious notation $\xi_s(Y) \;=\; \ln(Q_s^2(Y)/\Lambda), \xi(r) \;=\; \ln(1/(r^2\Lambda^2))$ and so on. Assuming that $\alpha_S(r) \;\ll\; \alpha_S(R)$ we obtain the following behaviour for the scattering amplitude in Iancu - Mueller approach:

$$\phi(Y-y,r)+\phi(y,R) \;\longrightarrow\; \phi(Y,r) \;+\; \frac{\alpha_S(\xi)}{2\,\pi}\,\left(-\,\xi_s^2(y_{min}) \;+\xi^2(R)\right)\;, \tag{4.69}$$

where y_{min} is defined by Eq. (4.68).

One can see that y_{min} depends on Y and, therefore, the asymptotic behaviour of the scattering amplitude cannot be calculated just using the Balitsky-Kovchegov equation on the contrary to our example with frozen α_S. On the other hand, for $\alpha_S(r) \;\ll\; \alpha_S(R)$ y_{min} is almost constant and the influence of the target is rather small.

These two examples illustrate the importance of understanding the argument in QCD the running coupling constant in the framework of the non-linear equation. In our simple model with Eq. (4.42) for the BFKL kernel the second example looks more reliable.

4.3 High energy scattering amplitude with the general BFKL kernel

The estimates discussed above are based on the solution to the non-linear Balitsky-Kovchegov equation given in Ref. [22]. In this section we are going to show that this solution cannot give a correct high energy asymptotic behaviour. In this section we use the full BFKL kernel and solve the Balitsky-Kovchegov equation in the saturation region.

4.3.1 The solution to the non-linear equation in the saturation region:

To search for the solution in the saturation region, we use several ideas and technical methods that have been discussed in Refs. [22, 13].

1. It is useful to consider the non-linear equation in a mixed representation, fixing impact parameter b, but introducing the transverse momenta as conjugated variables to the dipole sizes. The relations between these two representations are given by the following equations [13, 26]

$$N(r,y;b) \;\;=\;\; r^2\,\int_0^\infty kdk\,J_0(k\,r)\;\tilde{N}(k,y;b)\;; \tag{4.70}$$

$$\tilde{N}(k,y;b) \;\;=\;\; \int_0^\infty \frac{dr}{r}\;J_0(k\,r)\;N(r,y;b)\;; \tag{4.71}$$

2. In this representation the non-linear equation reduces to the form:

$$\frac{\partial\,\tilde{N}(k,y;b)}{\partial y} \;=\; \bar{\alpha}_S\,\Big(\,\chi(\hat{\gamma}(\xi))\,\tilde{N}(k,y;b) \;-\; \tilde{N}^2(k,y;b)\,\Big) \tag{4.72}$$

where $\chi(\hat{\gamma}(\xi)$ is an operator defined as

$$\hat{\gamma}(\xi) \;=\; 1 \;+\; \frac{\partial}{\partial\,\xi} \tag{4.73}$$

where $\xi \;=\; \ln(k^2\,k'^2\,b^4)$, and k and k' are the conjugated variables to the dipole sizes of the projectile and the target, b is an impact parameter which we assumed to be large in Eq. (4.72).

3. We expect there to be geometrical scaling behaviour of the scattering amplitude in the saturation domain. It means that $\tilde{N}(k,y;b)$ is a function of the single variable

$$z \;=\; \ln(Q_s^2(y,b)/\Lambda^2) \;-\; \xi(b) \;=\; \bar{\alpha}_S\,\frac{\chi(\gamma_{cr})}{1\,-\,\gamma_{cr}}\,(\,y\;-\;y_0\,)\;-\;\xi(b)\;; \tag{4.74}$$

where $\gamma_{cr} \;\approx\; 0.37$ is a solution of the equation [5, 24]

$$\frac{d\,\chi(\gamma_{cr})}{d\,\gamma_{cr}} \;=\; -\,\frac{\chi(\gamma_{cr})}{1\;-\;\gamma_{cr}}\;; \tag{4.75}$$

4. Introducing a function $\phi(z)$ we are looking for the solution of the equation in the form

$$\tilde{N}(z) \;=\; \frac{1}{2}\int^z\,d\,z'\,\Big(1\;-\;e^{-\,\phi(z')}\Big)\;; \tag{4.76}$$

5. We assume that function ϕ is a smooth function, such that $\phi_{zz} \;\ll\; \phi_z\,\phi_z$ where we denote $\phi_z = d\phi/dz$ and $\phi_{zz} = d^2\phi/(dz)^2$. This property allows us to rewrite

$$\frac{d^n}{(dz)^n}\,e^{-\phi(z)} \;=\; (-\phi_z)^n\,e^{-\phi(z)} \tag{4.77}$$

Substituting in Eq. (4.72) $\tilde{N}$ in the form of Eq. (4.76) and replacing y by $\hat{z}$ we obtain

$$\bar{\alpha}_S\,\frac{\chi(\gamma_{cr})}{1\;-\;\gamma_{cr}}\;\frac{d^2\tilde{N}(z)}{(dz)^2} \;=\; \bar{\alpha}_S\Big(\;[f\,\chi(1-f)\;-\;1]\,\tilde{N}(z)\;+\;\tilde{N}(z)\,e^{-\phi}\;\Big) \tag{4.78}$$

after taking the derivative with respect to z on both sides of Eq. (4.72). f denotes $f = d/dz$ in Eq. (4.78). An important property of function $f\,\chi(1-f)\;-\;1$, is the fact that at small f it has the expansion that starts [3] from f^2. Using Eq. (4.77) one can see that the first term on

[3] It should be stressed that the simplified model for $\chi(1-f) = \frac{1}{f(1-f)}$ does not have this property. This is an explanation why in Ref. [22] where this model was used, the solution was missed as we will discuss below.

r.h.s. of Eq. (4.78) is proportional to $e^{-\phi}$. Canceling $\bar{\alpha}_S\, e^{-\phi}$ on both sides of Eq. (4.78) and once more taking the derivative with respect to $\hat{z}$ we reduce Eq. (4.78) to the form:

$$\frac{\chi(\gamma_{cr})}{1\,-\,\gamma_{cr}}\,\frac{d^2\,\phi}{(dz)^2} \;=\; \left(1\;-\;e^{-\phi(z)}\right)\;-\;\frac{d\,L(\phi_z)}{d\,\phi_z}\,\frac{d^2\,\phi}{(dz)^2}\;; \tag{4.79}$$

$$L(\phi_z) \;=\; \frac{\phi_z\;\chi\,(1\;-\;\phi_z)\;-\;1}{\phi_z}\;; \tag{4.80}$$

The answer in the simple model given by Eq. (4.42) obtained in Ref. [22] corresponds to the simplified version of $\chi(1-f) = 1/f$. In this case the second term in Eq. (4.79) vanishes and the solution for large $\hat{z}$ is

$$\phi(\hat{z}) \;=\; \frac{1\,-\,\gamma_{cr}}{\chi(\gamma_{cr})}\,\frac{z^2}{2} \tag{4.81}$$

For the full BFKL kernel function $\frac{d\,L(\phi_z)}{d\,\phi_z}$ is negligibly small for small ϕ_z. However, $\frac{d\,L(\phi_z)}{d\,\phi_z}$ being small for $\phi_z\,<\,1$ has a singularity at $\phi\,\rightarrow\,1$ namely

$$\frac{d\,L(\phi_z)}{d\,\phi_z}\;\longrightarrow\;\frac{1}{(\,1\;-\;\phi_z\,)^2}\qquad\text{for}\qquad\phi_z\longrightarrow\;1$$

The solution given by Eq. (4.81) is controversial since it was obtained assuming that $\frac{d\,L(\phi_z)}{d\,\phi_z}$ is small but it leads to large ϕ_z where this term is essential. We can conclude that this solution is valid only in the simplified model with the kernel given by Eq. (4.42).

For the full BFKL kernel we can try an opposite approximation assuming that $\phi(z)$ is large ($\phi\;\gg\;1$) but ϕ_z is approaching to 1 at $z >> 1$. In vicinity $\phi_z = 1$ we reduce Eq. (4.79) to

$$\frac{1}{(1\;-\;\phi_z\,)^2}\;\frac{d^2\,\phi}{(d\hat{z})^2}\;=\;1. \tag{4.82}$$

For large z Eq. (4.82) has a solution

$$\phi(\hat{z}) \;=\; z\;-\;\ln z \tag{4.83}$$

which can be verified by explicit calculations. It should be stressed that $\phi(z)$ of Eq. (4.83) satisfies all conditions of a smooth function that has been used for the derivation of Eq. (4.79). We can also check that the l.h.s. of Eq. (4.79) is proportional to $1/z^2$ and it can be neglected.

It is more convenient to use the coordinate representation for the scattering amplitude (see Eq. (4.70) and Eq. (4.71)). We can simplify Eq. (4.71) in the saturation region where $N(r, y; b)$ manifests a geometrical scaling behaviour being a function of one variable $N(r^2 Q_s^2(y, b))$. The main contribution in this equation stems from the kinematic region: $k\,r\;<\;1$ and $r^2 Q_s^2\;>\;1$. Indeed, for $k\,r\;>\;1$ the integral of Eq. (4.71) is small, due to the oscillating behaviour of $J_0(k\,r)$ while for $r^2 Q_s^2 < 1$ the amplitude N being in the perturbative QCD domain is rather small. Therefore, Eq. (4.71) can be rewritten in the form:

$$\tilde{N}\,(k, y; b) \;=\; \tilde{N}\,(z) \;=\; \frac{1}{2}\int^{\hat{z}}\;d\,z' N(z') \tag{4.84}$$

where z' in the integral is defined by Eq. (4.47). Comparing Eq. (4.76),Eq. (4.83) and Eq. (4.84) one concludes that

$$N\left(r^2 Q_s^2(y,b)\right) \;=\; 1 \;-\; e^{-z(r)\;+\;\ln z(r)} \tag{4.85}$$

with $z(r)$ is defined by

$$z(r) \;=\; \ln(Q_s^2\, r^2) \;=\; \bar{\alpha}_S \frac{\chi(\gamma_{cr})}{1\;-\;\gamma_{cr}}\;(\,y\;-\;y_0\,)\;-\;\ln(1/r^2\Lambda^2)\;. \tag{4.86}$$

We are aware that the majority of experts, including one of us, have thought that solution of Eq. (4.81) gives a correct asymptotic behaviour for the scattering amplitude. Indeed, at first sight, the approach with the kernel of Eq. (4.42) is well motivated [22], while the same result can be derived without addressing any model for the kernel (see Ref. [1] and references therein). Function ϕ has a very transparent physical meaning (see Eq. (4.46)): $\exp^{-\phi}$ is a probability for a dipole to pass the target without any inelastic interaction. In the solution given by Eq. (4.81), $\exp^{-\phi}$ is the probability that no extra gluon could be emitted (see Fig. 8-a). However, this solution does not suppress the elastic scattering shown in Fig. 8-b. This diagrams can easily be calculated

$$N_{el} \;\propto\; \frac{1}{\pi\, r^2}\;\int_{Q_s^2}^{\frac{1}{r^2}}\;\frac{dq^2}{q^4}\;\left(\frac{q^2}{Q_s^2}\right) \;=\; e^{-z(r)\;+\;\ln z(r)} \tag{4.87}$$

where q^2/Q_s^2 describes the emission of the 'soft' gluon with $1/r < q < Q_s$ from the dipole with the typical size $1/Q_s$. Since N_{el} is the amplitude at fixed impact parameter we divided the cross section by the area of the scattering dipole. The idea that approaching to the black disc will be described by the Born approximation in the saturation region has been discussed [27] but we found that this asymptotic behaviour follows from the Balitsky-Kovchegov non-linear equation.

A kind of argument against could be the result of the numerical simulations for dipole-dipole scattering by Salam in Ref. [2] which supports Eq. (4.81), in spite of the fact that the general BFKL kernel has been used. In Fig. 9 we compare two solutions (Eq. (4.81) and Eq. (4.85)) with the numerical solution of the Balitsky-Kovchegov equation given in Ref.[28]. We fit the numerical solutions by two function:

$$N(z) \;=\; 1 \;-\; C_1^1\, e^{-C_2^1 z^2}\;; \tag{4.88}$$

$$N(z) \;=\; 1 \;-\; C_1^2\, e^{-(z-ln(z+C_2^2))}\;; \tag{4.89}$$

One can see that both formulae could describe the solution. Therefore, we cannot use the numerical solution as an argument in favour of any solution. It is interesting to mention that the value of C_2 in Eq. (4.88) ($C_2 = 0.11$) is closer to the theoretical value in Eq. (4.81) than it is found by Salam.

4.3.2 High energy amplitude in the saturation region:

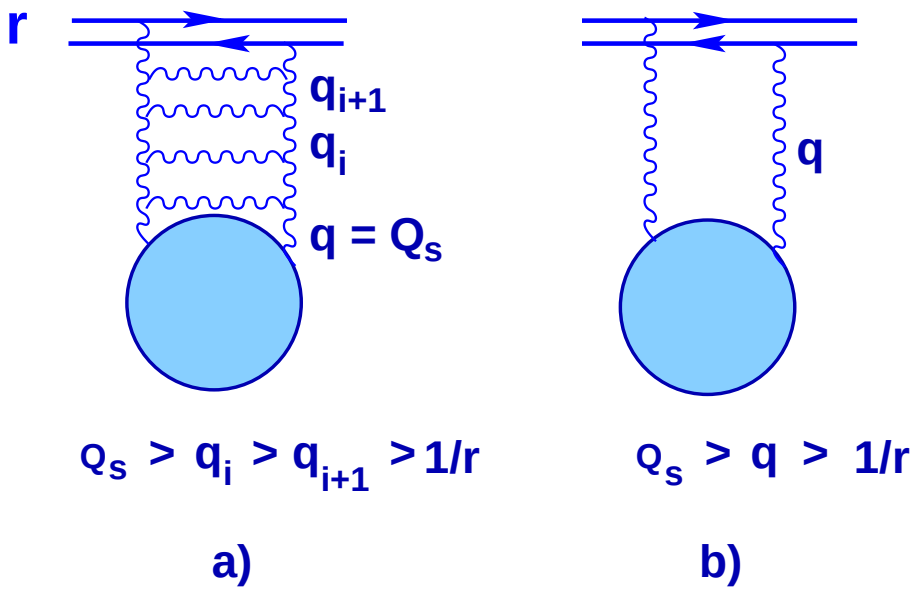

Figure 8: The gluon emission which is suppressed in the solution given by Eq. (4.81) (Fig. 8-a); and the elastic rescattering (Fig. 8-b) which is taken into account in the solution by Eq. (4.85) .

Fixed α_S :

We can calculate the scattering amplitude in the saturation region using the Iancu - Mueller factorization in the form of Eq. (4.53) but with the contour C_1 for integration over ν. For $N(Y-y,r,b;[\nu])$ we use Eq. (4.85) with z replaced by $z + 2\Phi[\gamma(r_i)]$ where Φ is defined in Eq. (4.52) and $z = \ln Q_s^2 - \ln(1/r^2)$. As in the case of the double log kernel we choose $\gamma(r_i) = \nu$ and $\gamma(r_i') = \tilde{\gamma}(r_i, r_i')/\nu$.

We can easily take the integral of Eq. (4.53) if we neglect the ν dependence in $\ln z$. In this case the product $N(Y-y,r,b[\nu]\, N(y,R,b;[\tilde{\gamma}(r_i,r_i')/\nu])$ does not depend on ν. This simple

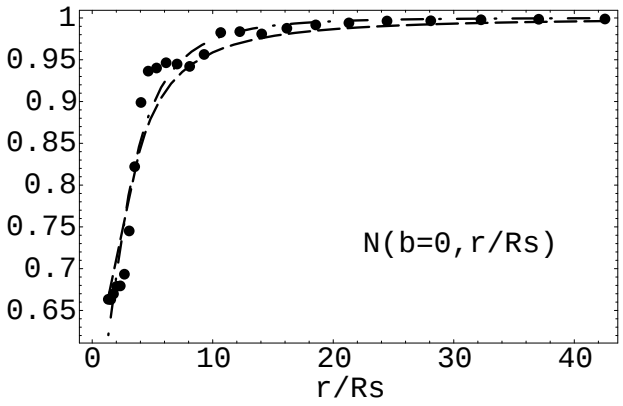

Figure 9: The fit of the numerical solution to the Balitsky-Kovchegov equation [28] using Eq. (4.88) and Eq. (4.89). The dashed line corresponds to Eq. (4.89) with $C_1^2 = 0.69$ and $C_2^2 = -1.05$ while the dashed-dotted line describes Eq. (4.88) with $C_1^1 = 0.25$ and $C_2^1 = 0.11$.

observation leads to the answer for the scattering amplitude

$$N\,(\,r,R,Y;b\,)\;=\;1\;-\;e^{-\,z(Y,r,R)+2\,\ln(z(Y,r,R)/2)} \tag{4.90}$$

where $z(Y,r,R)$ is given by Eq. (4.57).

As in the case of the simplified kernel of Eq. (4.42) , the main contribution stems from the set of enhanced diagrams.

Running α_S :

Calculating the diagram of Fig. 8-b for the running QCD coupling we obtain the answer

$$\phi(y,r)\;=\;\ln(r^2\,Q_s^2)\;-\;\ln\left(\ln\left(\frac{\ln(Q_s^2/\Lambda)}{\ln(1/(r^2\,\Lambda^2))}\right)\right) \tag{4.91}$$

with $Q_s \propto e^{\sqrt{cy}}$. We can also verify that Eq. (4.91) is the solution to the generalization of the equation of Eq. (4.72) with the prescription for running α_S given in Ref. [25].

This change leads to remarkable consequences. Indeed, since the minimal value of $Z(Y-y,r)\,+\,Z(y,R)$, where $Z(y,R)\;\ln(Q_s^2(y)\,R^2)$, occurs at $y\,=\,0$ or $Y-y\,=\,0$ the resulting amplitude in the saturation region is

$$N\,(\,r,R,Y;b\,)\;=\;1\;-\;e^{-\,\ln(Q_s^2(Y)/\Lambda^2)+\ln(R^2/r^2)} \tag{4.92}$$

For simplicity, we did not write in Eq. (4.92) the $\ln\ln(\ldots$ in Eq. (4.92).

Therefore, the asymptotic behaviour of the scattering amplitude for running α_S is determined by the non-linear equation [3, 4], which is able to describe the colour glass condensate phase of QCD [8] in this case.

5 Conclusions

In this paper we showed that the Iancu-Mueller factorization [1] is closely related to a sum of a particular set of enhanced diagrams (see Fig. 6) in the Reggeon -like diagram technique based on the BFKL Pomeron. This set of diagrams leads to the high energy scattering amplitude in wide range of energy and/or Bjorken x, namely

$$Y=\ln(1/x)\;<\;\frac{1}{\bar{\alpha}_S}\,\ln\,\frac{N_c^2}{\bar{\alpha}_S}\;. \tag{5.93}$$

We found a simple formula of Eq. (4.53) which sums these diagrams and manifests the Iancu-Mueller factorization. Using this formula we confirm the Iancu-Mueller result, that at fixed QCD coupling, the high energy asymptotic behaviour is determined by the enhanced

diagrams, but not by the 'fan' diagrams that are summed by the means of Balitsky-Kovchegov non-linear equation. We showed that the dipole -dipole amplitude in the saturation region can be written as

$$N(r,R;Y) \;=\; 1 - \Big(N^{BK}(r,R;Y) - 1 \Big)^{\frac{1}{2}} \;\; . \tag{5.94}$$

However, for the running QCD coupling the main contribution in the saturation region stems from the 'fan' diagrams of Fig. 2-a (or Fig. 5) -type. This new result allows us to penetrate the saturation region, summing the 'fan' diagrams of more general type (see Fig. 2-b for the first such diagram). The first suggestion of how to sum such diagrams was proposed in Ref. [14], and the present paper confirms our hope that the general 'fan' diagrams will lead to the estimates of high energy asymptotic behaviour for running QCD coupling in the saturation region.

Our final result for the asymptotic behaviour of the scattering amplitude is quite different from that in the Iancu - Mueller paper [1] even for fixed QCD coupling case. This difference stems from the new solution to the non-linear equation found in this paper, which includes the general BFKL kernel as opposed to the simplified version of the kernel (see Eq. (4.42)) which has been used in Ref. [22].

Our approach to the Iancu-Mueller factorization is even closer to the Monte Carlo simulation than the original papers [1], and the semi-analytical estimates suggested in Ref. [2]. We hope that the simple formula suggested in this paper will give an impetus for searching for a new approach to find the high energy amplitude in the saturation region. We believe that we have demonstrated in this paper, that the Iancu-Mueller factorization provides a method to take the essential fluctuations in the partonic wave function of colliding dipoles into account and shows the practical method of calculation beyond of the non-linear equation. It also allows us to find the region of applicability of the non-linear equation.

Acknowledgments

We thank E. Gotsman, U. Maor and A. Mueller for fruitful and stimulating discussions on the subject of this paper. We are specially grateful to A. Mueller that he drew out attention to his ideas on how to include the QCD running coupling constant in the non-linear equation [25].

E.L. is indebted to the Alexander-von-Humboldt Foundation for the award that gave him a possibility to work on low x physics during the last year.

This research was supported in part by the Israel Science Foundation, founded by the Israeli Academy of Science and Humanities.

References

[1] E. Iancu and A. H. Mueller, *Nucl. Phys.* **A730** (2004) 460, 494, [arXiv:hep-ph/0308315],[arXiv:hep-ph/0309276].

[2] A. H. Mueller and G. P. Salam, *Nucl. Phys.* **B475** (1996) 293 [arXiv:hep-ph/9605302]; G. P. Salam, *Nucl. Phys.* **B461**, 512 (1996) [arXiv:hep-ph/9509353].

[3] Ia. Balitsky, *Nucl. Phys.* **B 463** (1996) 99.

[4] Yu. Kovchegov, *Phys. Rev.* **D 60** (2000) 034008.

[5] L. V. Gribov, E. M. Levin and M. G. Ryskin, *Phys. Rep.* **100** (1983) 1.

[6] A. H. Mueller and J. Qiu, *Nucl. Phys.* **B 268** (1986) 427.

[7] L. McLerran and R. Venugopalan, *Phys. Rev.* **D 49** (1994) 2233, 3352; **D 50** (1994) 2225, **D 53** (1996) 458, **D 59** (1999) 09400.

[8] J. Jalilian-Marian, A. Kovner, L. McLerran, and H. Weigert, *Phys. Rev.* **D 55** (1997) 5414; J. Jalilian-Marian, A. Kovner, and H. Weigert, *Phys. Rev.* **D 59** (1999) 014015; J. Jalilian-Marian, A. Kovner, A. Leonidov, and H. Weigert, *Phys. Rev.* **D 59** (1999) 034007, Erratum-ibid. *Phys. Rev.* **D 59** (1999) 099903; A. Kovner, J.Guilherme Milhano, and H. Weigert, *Phys. Rev.* **D 62** (2000) 114005; E. Ferreiro, E. Iancu, A. Leonidov and L. McLerran, *Nucl. Phys.* **A703** (2002) 489; E. Iancu, A. Leonidov and L. D. McLerran, *Phys. Lett.* **B510** (2001) 133, *Nucl. Phys.* **A692** (2001) 583; E. Iancu and L. D. McLerran,*Phys. Lett.* **510** (2001) 145; H. Weigert, *Nucl. Phys.* **A 703** (2002) 823.

[9] E. Iancu and R. Venugopalan, *"The color glass condensate and high energy scattering in QCD,"* arXiv:hep-ph/0303204.

[10] E.A. Kuraev, L.N. Lipatov and V.S. Fadin, *Sov. Phys. JETP* **45** (1977) 199;
Ia.Ia. Balitsky and L.N. Lipatov,*Sov. J. Nucl. Phys.* **28** (1978) 822;
L.N. Lipatov, *Sov. Phys. JETP* **63** (1986) 904.

[11] M. Braun, *Eur. Phys.J.* **C16** (2000) 337; **C6** (1999) 343; M. A. Braun and G. P. Vacca, *Eur. Phys. J.* **C6** (1999) 147.

[12] M. G. Ryskin, Plenary talk at DIS'2003, 23 - 27 April, St.Petersburg, Russia.

[13] S. Bondarenko, M. Kozlov and E. Levin, *Nucl. Phys.* **A727** (2003) 139 [arXiv:hep-ph/0305150].

[14] E. Levin and M. Lublinsky, *"A linear evolution for non-linear dynamics and correlation in realistic nuclei"*, *Nucl. Phys.* **A** *(in press)*, arXiv:hep-ph/0308279.

[15] A. H. Mueller, *Nucl. Phys.* **B437** (1995) 107 [arXiv:hep-ph/9408245].

[16] E. Levin, *Phys. Rev.* **D49** (1994) 4469.

[17] G. Veneziano, *Phys. Lertters* **52B** (1974) 220; *Nucl. Phys.***B74** (1974) 365; M. Ciafaloni, G. Marchesini anf G. Veneziano, *Nucl. Phys.* **B98** (1975) 493.

[18] E. Laenen and E. Levin, *Nucl. Phys.*, **B451** (1995) 207 [arXiv:hep-ph/9503381]

[19] L. N. Lipatov,*Sov. Phys. JETP* **63** (1986) 904.

[20] J. Bartels, J. R. Forshaw, H. Lotter, L. N. Lipatov, M. G. Ryskin and M. Wusthoff, *Phys. Lett.* **B348** (1995) 589 [arXiv:hep-ph/9501204].

[21] H. Navelet and R. Peschanski, *Nucl. Phys.* **B634** (2002) 291 [arXiv:hep-ph/0201285]; *Phys. Rev. Lett.* **82** (1999) 137,, [arXiv:hep-ph/9809474]; *Nucl. Phys.* **B507** (1997) 353, [arXiv:hep-ph/9703238] A. Bialas, H. Navelet and R. Peschanski, *Phys. Rev.* **D57** (1998) 6585; R. Peschanski, *Phys. Lett.* **B409** (1997) 491.

[22] E. Levin and K. Tuchin, *Nucl. Phys.* **B573**, (2000) 833 [arXiv:hep-ph/9908317]; **A691**, (2001) 779 [arXiv:hep-ph/0012167]; **A693** (2001) 787 [arXiv:hep-ph/0101275].

[23] J. Kwiecinski and A. M. Stasto, *Acta Phys. Polon.* **B33** (2002) 3439; *Phys. Rev.* **D66** (2002) 014013 [arXiv:hep-ph/0203030]; A. M. Stasto, K. Golec-Biernat and J. Kwiecinski, *Phys. Rev. Lett.* **86** (2001) 596 [arXiv:hep-ph/0007192]; J. Bartels and E. Levin, *Nucl. Phys.* **B387** (1992) 617; E. Iancu, K. Itakura and L. McLerran, *Nucl. Phys.* **A708** (2002) 327 [arXiv:hep-ph/0203137].

[24] A. H. Mueller and D. N. Triantafyllopoulos, *Nucl. Phys.* **B640** (2002) 331 [arXiv:hep-ph/0205167]; D. N. Triantafyllopoulos, *Nucl. Phys.* **B648** (2003) 293 [arXiv:hep-ph/0209121].

[25] A. H. Mueller, *Nucl. Phys.* **B643** (2002) 501 [arXiv:hep-ph/0206216].

[26] S. Munier and R. Peschanski, *Phys. Rev.* **D69** (2004) 034008 [arXiv:hep-ph/0310357].

[27] E. M. Levin and M. G. Ryskin, *Phys. Rept.* **189** (1990) 267.

[28] E. Gotsman, M. Kozlov, E. Levin, U. Maor and E. Naftali, *"Towards a new global QCD analysis: Solution to the non-linear equation atarbitrary impact parameter,"* arXiv:hep-ph/0401021.